Proceedings 10th NUMGE 2023
10th European Conference on Numerical Methods in Geotechnical Engineering
Zdravkovic L, Kontoe S, Taborda DMG, Tsiampousi A (eds)

https://doi.org/10.53243/NUMGE2023-436

Micro-inspired constitutive modelling of clays

A. Amorosi

Department of Structural and Geotechnical Engineering, University of Roma "La Sapienza", Rome, Italy

ABSTRACT: Clays are ubiquitous in geotechnical and environmental engineering applications and understanding their complex mechanical behaviour is essential for designing and constructing safe and efficient structures. Over the years, numerous constitutive models have been developed to describe their mechanical behaviour, but only few of them were formulated in light of the complex microstructural features of these materials.
The aim of this paper is that of providing an overview of some recent advances in micro-inspired constitutive modelling of clays. After a review of multi-scale experimental evidence and its possible interpretation and generalisation in terms of internal variables controlling the mechanics of clayey soils, two examples of constitutive models are proposed, both developed in the framework of Thermodynamics with Internal Variables. This theoretical framework proves to effectively allow the development of constitutive models that not only respect the fundamental principles of thermodynamics, but also directly benefit of our understanding of the complex micromechanics of clayey soils.

Keywords: Porosity; Fabric; Clay; Constitutive modelling; Thermodynamics

1 INTRODUCTION

Soil mechanics is a well-established discipline that has always put considerable emphasis on the physical characteristics of the studied materials, whose peculiarity lies in their granular and multi-phase nature.

In fact, each series of introductory lectures at University level qualitatively emphasises the substantial role played by individual grains and, when present, their aggregates on the behaviour of the overall soil skeleton, highlighting the intricacy of the multi-physical interactions occurring at the micro-scale. These latter interactions increase as the grain size decreases, reaching the highest complexity in clayey soils.

Unfortunately, this premise often leads to a potential disappointment of the same class of students when they are first introduced to the mechanical behaviour of soils in general, and of clays in particular, at the continuum level, as most of the microstructural features previously discussed are only marginally considered in such a quantitative context, erroneously implying that the micro and macro scales are broadly independent. This is obviously not true, as shown by the huge amount of research carried out in this field. In fact, several research attempts aimed at linking microscopic features to macroscopic patterns of behaviour have characterised the whole history of soil mechanics (e.g. Mitchell, 1956; Smart, 1969; Smart and Tovey, 1982; Terzaghi, 1948), proposing either qualitative or, more recently, quantitative means to bridge the gap between scales.

This paper firstly aims to summarise some experimental evidence on the role of the microstructural characteristics of clayey soils on their mechanical behaviour, in order to provide a guide to the selection of relevant internal variables, i.e. state variables that condense microscopic mean characteristics and make them suitable to be incorporated into a macroscopic constitutive modelling framework. In light of the above, the specific modelling approach based on Thermodynamics with Internal Variables (TIV) (e.g. Maugin and Muschik, 1994) is then outlined and specialised to the case of clays, illustrating some recently obtained results.

2 EXPERIMENTAL EVIDENCE

Two fundamental clays microstructure descriptors are here considered: porosity and fabric.

As will be shown in the following, they are natural candidates to play the role of internal variables, given their substantial influence on the macroscopic mechanics of clays, their evolving character, and their property of being in principle measurable but not controllable at each stage of their evolution.

Porosity and fabric share some common features. One is the scale dependency, which leads to different pictures depending on the scale adopted in the observation. Another one consists in the nowadays strong technological constraints that limit direct experimental observations at the microscale only to *post-mortem* conditions, i.e. at the end of any test, thus limiting our capability to follow their evolution *in-situ*, which, in the jargon adopted by the multi-scale experimental community, means "during the test".

2.1 Porosity

The classical definition of porosity n adopted in soil mechanics refers to the ratio of the volume of voids to the total volume of the macroscopic soil element. Equivalent scalars are alternatively adopted to express related measures, as the specific volume v or the void ratio e. The above mean variables can be evaluated by standard mass-volume relationships.

The careful observation of thin sections of a clayey sample by scanning electron micrography (SEM) reveals a more complex picture of the microstructure and its articulate patterns in terms of porosity: in fact, as originally proposed by Olsen (1962) and Barden and Sides (1970) and then confirmed by many others (e.g. Delage and Lefebvre, 1984; Hattab et al, 2013; Hicher et al. 2000), the material can be schematised as composed by an aggregated microstructure in which larger pores characterise the inter-aggregate volumes, while smaller ones are observed within the aggregate (intra-aggregate pores). This is confirmed by mercury intrusion porosimetry (MIP) data, often showing bimodal patterns in the pore size distribution curves, especially with reference to soft natural or reconstituted clays. Although both SEM and MIP techniques are subjected to continuous improvements in terms of accuracy and reliability, comparing measurements of pore size distributions obtained by them does not always lead to the same outcome, as discussed in Zheng et al. (2022).

In spite of these limitations, it is possible to trace the mechanically induced evolution of porosity at different scales by interrupting any geotechnical test, cutting the sample in a representative number of portions and, after drying, subjecting them to SEM and MIP measurements. This procedure has been applied to both reconstituted and intact clays, characterised by different minerology, while being subjected to either radial compression paths, as the isotropic or oedometric ones, or to deviatoric tests (e.g. Chow et al., 2019; Gao et al., 2020; Guglielmi et al., 2022; Hattab and Fleureau, 2010; Hicher et al., 2000; Mitaritonna et al., 2014; Yu et al., 2016; Zheng et al., 2022).

The above observations can be used to sketch a simplified interpretation of the microscopic response of a sample of reconstituted clay subjected to virgin radial compression, just after its transition from slurry to solid state, up to low to medium effective stresses: it mainly experiences a volume reduction of the inter-aggregate pores, which corresponds to the macroscopic evolution of the mean porosity as expressed by n or v, while intra-aggregate ones remain almost unchanged (e.g. Guglielmi et al., 2022; Zhang et al, 2022). Similarly, during triaxial drained tests, the shearing process alters the size of the inter-aggregate pores, leaving the intra-aggregate ones almost unchanged (Yu et al., 2016). This pattern supports the findings numerically obtained by Anandarajah (2000a,b), indicating that, at least for the idealised clays investigated by the Author, the mechanical behaviour depends on the aggregate-to-aggregate interactions, rather than on the particle-to-particle ones. Some Authors also infer that, especially in non-active clays, the aggregate-to-aggregate interaction is mainly characterised by frictional contacts in which the surface-related electro-chemical forces are negligible (Chang et al., 2009; Yu et al., 2016), while others (Hattab and Chang, 2015; Pedrotti and Tarantino, 2018) provide a more articulate picture in which non-contact forces play a role in the mechanical behaviour of the investigated clayey soil.

It should be remarked that the general interpretation in terms of double porosity provided above holds until a relatively high level of stress is attained: at that stage inter-aggregate pores exhibit a size comparable to that of the intra-aggregate ones, leading to a unimodal pore size distribution, whose mean value turns out to be the one controlling the behaviour of the soil (Guglielmi et al., 2022).

The microstructural insight summarised above appears to be consistent with the well-established Critical State Soil Mechanics framework (CSSM), which first considered the fundamental role of the porosity, via v, on each aspect of the mechanical behaviour of clays, thus extending the set of state variables that up to that moment had been limited to the sole effective stress state. In this framework the irreversible variation of the void ratio, as read on the virgin compression line, controls the evolution of the mechanics of the material leading, in an elasto-plastic setting, to the isotropic volumetric hardening law of the Cam-Clay family of constitutive models.

2.2 Fabric

In granular mechanics, the term fabric refers to the orientation-related characteristics of the material at the grain scale. In clays, given their aggregated microstructure, it is possible to define different fabrics with reference to different scales: for observations carried out at the scale of about 1 μm, i.e. roughly corresponding to the single particle dimension, the fabric will be representative of the intra-aggregate, while the orientation pattern emerging at the scale of tens of microns should be interpreted as that of the aggregates.

In mechanics the quantitative description of fabric is condensed in a tensorial entity named fabric tensor (Fu and Dafalias, 2015; Kanatani, 1984) which, in the following, will be restricted to second order. In its original formulation, the fabric tensor is defined as:

$$\mathbf{F} = \frac{1}{N}\sum_{k=1}^{N} \mathbf{n}^k \otimes \mathbf{n}^k \tag{1}$$

where N is the number of the particles/aggregates being quantified in the domain, $\mathbf{n}$ is the direction-related unit vector, $\otimes$ is the tensor product and the superscript k

refers to the *k*th grain/aggregate. In principle, once the scale of observation is set, it is possible to identify the direction $\mathbf{n}^k$ of each particle/aggregate in the reference volume so to define the overall directional probability density function and calculate, by Equation (1), the corresponding fabric tensor **F**, which is characterised by a normalised trace. Assuming the observation is carried out in 2D, as costumary for SEM-based images, the second order fabric tensor reduces its degrees of freedom to two, i.e. it can be fully described by two scalar values: 1) the major principal direction (typically expressed by an angle with respect to a fixed reference in the plane of analysis), which represents the predominant orientation of the *N* particles/aggregates and 2) a relation between its two principal components F_1 and F_2, such as F_1/F_2 or F_1-F_2, related to the degree of anisotropy or, in other terms, to the scatter of the directional distribution with respect to its major principal direction defined in 1).

Alternative but equivalent definitions have been proposed in the past and are often adopted in the interpretation of SEM images: among them, it is worth recalling here that outlined in the approach proposed by Martinez-Nistal et al. (1999). It requires a digital processing of the SEM image at the relevant scale, by the analysis of the brightness intensity of the pixels. At this stage, elongated bright regions in the image are interactively thinned to line-shaped regions. These are processed through filtering to derive, based on a brightness threshold, a binary image in which lines complying with the threshold are considered of interest. These are thinned to a pixel width and the fabric orientation is calculated from the texture line map using a line-following algorithm to obtain polygonal lines, whose segments are logged in terms of length and orientation (vectors). A rose histogram is then used to represent the vector lengths l_i, for each direction range, θ_i (interval 10°). A statistical analysis of the vector lengths results in both the mean direction of all the vectors θ, and a scalar statistical expression of the dispersion of the vectors with respect to the mean direction $\overline{L}$:

$$\theta = tan^{-1}\left[\frac{\sum_{i=1}^{n} l_i sen\theta_i}{\sum_{i=1}^{n} l_i \cos\theta_i}\right] \tag{2}$$

$$L = \sqrt{\left(\sum_{i=1}^{n} l_i \cos\theta_i\right)^2 + \left(\sum_{i=1}^{n} l_i \sin\theta_i\right)^2} \tag{3}$$

$$\overline{L} = \frac{L}{\sum_{i=1}^{n} l_i} \tag{4}$$

Given the expression of $\overline{L}$, its values characterising different degrees of orientation are not of uniform size:

$\overline{L}$ =1: maximum degree of iso-orientation;
0.21 < $\overline{L}$ < 1: highly oriented fabric;
0.15 < $\overline{L}$ < 0.21: low oriented fabric;
$\overline{L}$ < 0.15: random oriented fabric.

Quantitative evaluation of the directional patterns at the microscale and their evolution during triaxial radial compression and/or shearing have been presented, among others, by Cetin (2004), Cotecchia and Chandler (1998), Hattab and Floreau (2010), Hicher et al. (2000), Mitaritonna et al. (2014). All the above studies indicate that the previously experienced virgin compression, if sufficiently extended, leads to a consistently oriented microstructure. This is, for example, the case of reconstituted clayey samples initially compressed in a consolidometer from their slurry state, leading to an orientation pattern at the microscale that is consistent with the imposed 1D compression conditions. If the same material is then subjected to a sufficiently extended isotropic virgin compression, it smoothly modifies the orientation of its components towards a more dispersed (i.e. less oriented) conditions. The picture becomes less clear when imposing deviatoric paths up to failure: in fact, localisation often occurs, implying the coexistence, within the same specimen, of rather different orientation patterns at the microlevel.

Just like what discussed for porosity, the above references confirm that the quantitative description of fabric at the scale of about 1 μm, i.e. roughly corresponding to the single particle dimension, provides a picture that can be rather different, and often less significative, from that emerging with respect to the scale of tens of microns, i.e. that of the aggregates, at least for relatively soft natural and reconstituted clays. In fact, the careful observation of fabric during virgin radial stress paths highlights that the key processes are occurring at this latter scale, where the aggregates exhibit a well-defined directional evolution, not necessarily accompanied by a comparably evident evolution of the intra-aggregate particle orientations (e.g. Mitaritonna et al., 2004). This picture is consistent to that provided by Anandarajah (2000a,b) in his pioneering attempt to model the behaviour of clays by a DEM approach.

The macroscopic effect of the orientational patterns discussed above is anisotropy. This crucial aspect of the mechanics of soils, in general, and clays in particular, affects the full range of their mechanical behaviour, including the reversible elastic behaviour, as detected by very small stress–strain perturbations (e.g. Pennington et al., 1997; Zdravkovic and Jardine, 1997) and the irreversible plastic response, as for the orientation of the

yield domain in the stress space resulting from careful probing from the in-situ state (Callisto and Calabresi, 1998; Kim and Finno, 2012; Smith et al., 1992), up to the response at critical state, as discussed in Li and Dafalias (2012).

Both elastic and plastic anisotropy of clayey soil display an evolving character when the material is subjected to sufficiently extended radial stress paths (e.g. Gens, 1982; Mitaritonna et al., 2014). In fact, they seem to evolve in a consistent way, being the plausible macroscopic manifestation of clay's internal evolving microstructure. This common physical basis supports the idea of introducing a unique tensorial variable in the constitutive modelling of clays at the macroscopic level, capable of accounting for all the above discussed directional properties as suggested in Amorosi et al. (2021) within the framework of elasto-plasticity, along the line of the pioneering work of Hueckel and Tutumluer (1994). Essentially, it was proposed to combine anisotropic hardening laws, describing the evolution of a fabric tensor-related variable controlling the distortion of the yield domain in the stress space (e.g. Dafalias, 1986; Kavvadas, 1982) with corresponding elastic formulations also dependent on a second order tensor related to the fabric one. This perspective is further developed in a different theoretical framework in the final part of this contribution.

3 WAVE PROPAGATION AS A PROXY FOR CLAY MICROSTRUCTURE

In this paragraph the key results emerging from Mitaritonna et al. (2014) are summarised, aiming at providing a picture of the evolving microstructural features of a reconstituted clay, as observed during laboratory experiments, and their relation with the evolving reversible response, as detected propagating shear waves polarised along different planes. The objective is to demonstrate the link between these two different aspects, highlighting the great potential of wave propagation to indirectly acquire average information on porosity and fabric, thus allowing to carry out *in-situ* observations, i.e. during a test, rather than limiting the microstructural data acquisition to the *post-mortem* stages.

Mitaritonna et al. (2014) propose a series of tests carried out on reconstituted Lucera clay, a mainly illitic medium plasticity clay of marine origin. Triaxial tests were performed by stress-controlled systems fitted with horizontal multi-directional bender elements. The testing programme was designed to investigate the evolution of clay stiffness in general and stiffness anisotropy in particular, this latter described by the ratio G_{hh}/G_{hv}, along constant stress ratio virgin compression paths attaining mean effective stresses much higher (up to $p' \approx 1350$ kPa) than those previously imposed in a consolidometer ($p' \leq 70$ kPa) and, at some stages, also imposing unloading-reloading branches. The values of the stress ratio $\eta = q/p'$ applied in the different tests ranged from 0 to 0.8, as illustrated in Figure (1). Only two tests (4 and 5) were characterised by a variation of the consolidation stress ratio, while all the others were carried out at constant η. Thin vertical sections of the specimens were prepared, either at the end of the consolidometer stage or of the triaxial radial compression paths, to be then analysed by SEM at the scale of the tens of microns, i.e. corresponding to the aggregates one, quantitatively elaborating the images by the approach proposed by Martinez-Nistal et al. (1999).

The observed values of G_{hh}/G_{hv} at the equilibrium states during the stress paths tests are plotted versus p' in Figure (2), where the stiffness ratios, measured at normally consolidated equilibrium states along the different constant-η compression paths, are joined with different curves.

For p' values below the consolidometer-preconsolidation pressure, i.e. for initially overconsolidated states, all the different test data are located on about a single horizontal line, corresponding to $G_{hh}/G_{hv} \approx 1.12$-$1.13$; this observation suggests that up to this stress level the shear stiffness ratio is not significantly influenced by the differences in stress ratio η applied in the recompression of the clay. Therefore, in its initial overconsolidated state, the clay is characterised by a stiffness anisotropy ratio $G_{hh}/G_{hv} \approx 1.12$. This value is related to the directional character developed by the clay microstrucure during one-dimensional consolidation from slurry in the consolidometer: in fact, the digital process of the corresponding SEM pictures indicates an average direction $\theta = 32°$ with respect to the horizontal one and a degree of anisotropy $\overline{L} = 0.28$, corresponding to a highly oriented fabric (Figure (5a)).

When further radially compressed beyond its initial yield stress, the stiffness ratio either decreases, as in tests 1 and 2, or increases, as in tests 4 and 5, prior to reaching a constant value, at about $p' \approx 350$ kPa, which depends on the imposed stress ratio η.

During test 3, corresponding to $\eta = 0.6$, the anisotropy ratio is always about $G_{hh}/G_{hv} \approx 1.11$, a value close to the post-consolidometer one. This is consistent with the hypothesis that the stress ratio the soil was subjected to in the 1D compression in the consolidometer was equal to that applied in test 3, $\eta = 0.6$, due to a $K_0 = 0.56$, as predicted by Jaky (1944), for the clay under study. In fact, at the end of test 3 the SEM image, shown in Figure (5), indicates a degree of anisotropy, $\overline{L} = 0.27$, very similar to the initial one and a lower mean direction $\theta = 7°$, which highlights the further microstructural reorientation experienced by the material along the persistent K_0 conditions imposed in the triaxial system. A careful inspection of the SEM images indicates that during test 3 the most relevant microstructural modification consists in the reduction of the interaggregate pores in the virgin compression stages, on average characterised by

an initial equivalent diameter of about 10 μm, then reducing to 5 μm at the end of the test. This is confirmed by the conventionally evaluated specific volume v, which varies along the virgin compression line (Figure (3)): as expected, upon the unloading-reloading stages, v experiences minor changes, fully recovered when back on the virgin compression line. Figure (4) shows the evolution of G_{hv} and G_{hh} against p' in a bi-log plot, clearly highlighting the well-known dependence of the elastic stiffness moduli on the current effective stress state and on the previously experienced virgin stress-strain history. In fact, along each unloading-reloading branch, i.e. for each attained value of the preconsolidation pressure p'_o and/or the corresponding specific volume v read on the virgin compression line, the moduli vary non-linearly with p'; when subjected to further compression along the virgin compression line, thus inducing permanent variation of the specific volume, the clay experiences an irreversible modification of its microstructure in terms of porosity which affects the subsequent stiffness measurements, leading to augmented G_{hv} and G_{hh} values, as observed along the following unloading-reloading branches.

Compression paths characterised by stress ratio $\eta = 0$ (test 1) and 0.3 (test 2), lower than the initial $\eta = 0.6$, induce a permanent reduction in the degree of anisotropy, leading to $G_{hh}/G_{hv} \approx 1.05$ for $\eta = 0.3$ and about 1.01 for $\eta = 0$. This is confirmed by the analysis of the SEM image shown in Figure (5b), obtained at the end of test 2, characterized by a mean direction $\theta = 5°$ and $\overline{L} = 0.13$, typical of a randomly oriented fabric.

On the contrary, the anisotropy ratio increases up to 1.22 during test 4, where the soil was mostly compressed along the highest ratio $\eta = 0.8$. Even this evidence finds its microstructural confirmation in the results of the analysis of the SEM image shown in Figure (7), referred to the end of test 4, where $\theta = 2°$ and $\overline{L} = 0.37$, corresponding to a very oriented fabric. It is worth noting that in test 4 the stress ratio η has been decreased from 0.8 to 0.1 at p' = 700 kPa and then compressed at constant $\eta = 0.1$ up to p' = 1350 kPa. Figure (2) shows that the anisotropy ratio reduces only slightly (from 1.22 to 1.21) along the new η path. This observation suggests that the anisotropy induced in the material by constant-η compression up to relatively high pressures (p' = 700 kPa in this case) can be modified by further compression under different η values only when reaching effective stress levels larger than twice those previously applied along the initial η-constant path. To corroborate this evaluation, a similar test was carried out, during which the stress ratio was reduced from 0.8 to 0.1 at p' = 350 kPa and then compression at $\eta = 0.1$ was further developed, up to p' = 1350 kPa (Test 5). In this case, a progressive reduction of the shear stiffness ratio, down to a value of 1.15 is recorded. The results of tests 4 and 5 lead to the conclusion that a change in degree of shear stiffness anisotropy is possible when η varies, although it requires large plastic straining, as a small amount of irreversible deformation under the new η is not sufficient to significantly modify the previously acquired directional character of the soil. This conclusion is consistent with what suggested by Lewin (1973) in his pioneering work on the evolving character of the plastic potential of clays: a different, though related, aspect of the mechanics of clay.

In brief, for an approximately constant fabric configuration of the clay, as in test 3, the reversible response of the reconstituted Lucera clay varies - non linearly - with the effective stress state and the specific volume read on the virgin compression line at the preconsolidation pressure, this latter reflecting the microstructural configuration of the material in terms of porosity. Permanent changes in porosity, induced by further compression of the specimen along the virgin compression line, are mirrored in a scaling factor that equally affects both stiffness moduli G_{hv} and G_{hh}. On the other hand, if the clay experiences differently oriented virgin radial stress-strain paths, sufficiently extended to induce a microstructural modification in terms of fabric, this reflects into a modification of the stiffness anisotropy making the reversible behaviour of the soil not only dependent on the current effective stress state and (virgin compression-related) porosity but also on the fabric tensor which accounts for the mean microscopic directional properties of the clay at the macroscopic level.

In conclusion, the above evidence clearly shows the intimate relationship between the micro-features of a reconstituted clay in terms of porosity and fabric and its reversible macroscopic response, observed through the propagation of polarised waves along different planes, providing a means to gain indirect insight into the microscopic patterns of the material while conducting laboratory tests, i.e. while exploring its macroscopic behaviour at different states.

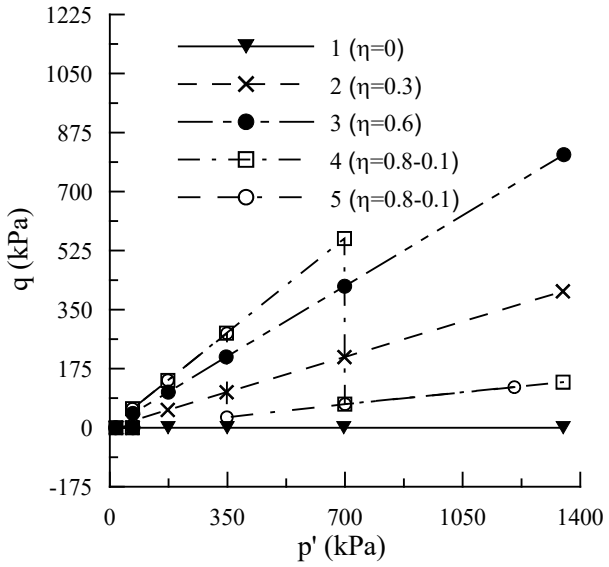

Figure 1. Testing programme (Mitaritonna et al., 2014)

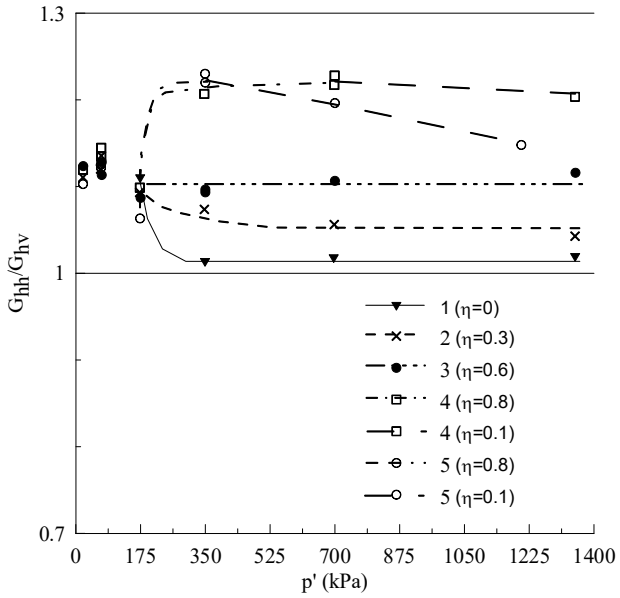

Figure 2. Shear stiffness anisotropy evolution

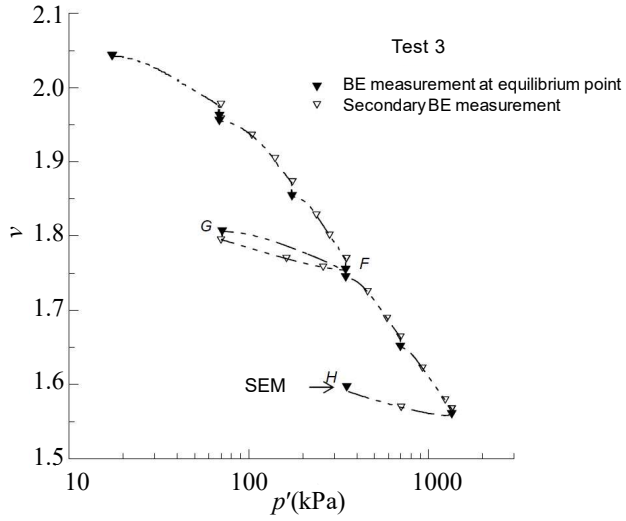

Figure 3. Test 3: compressibility plot and BE measurements

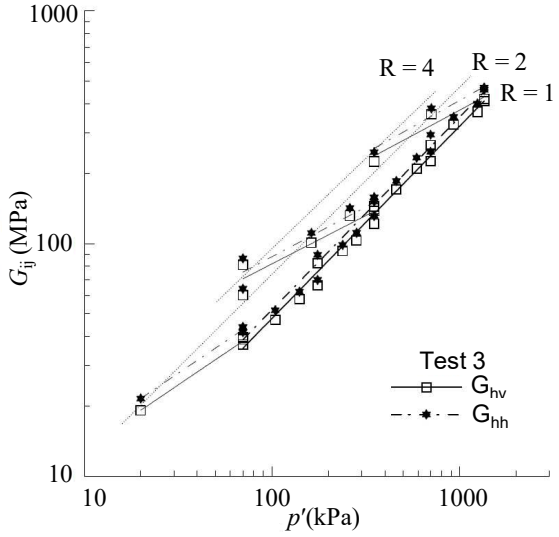

Figure 4. Evolution of G_{hv} and G_{hv} during test 3

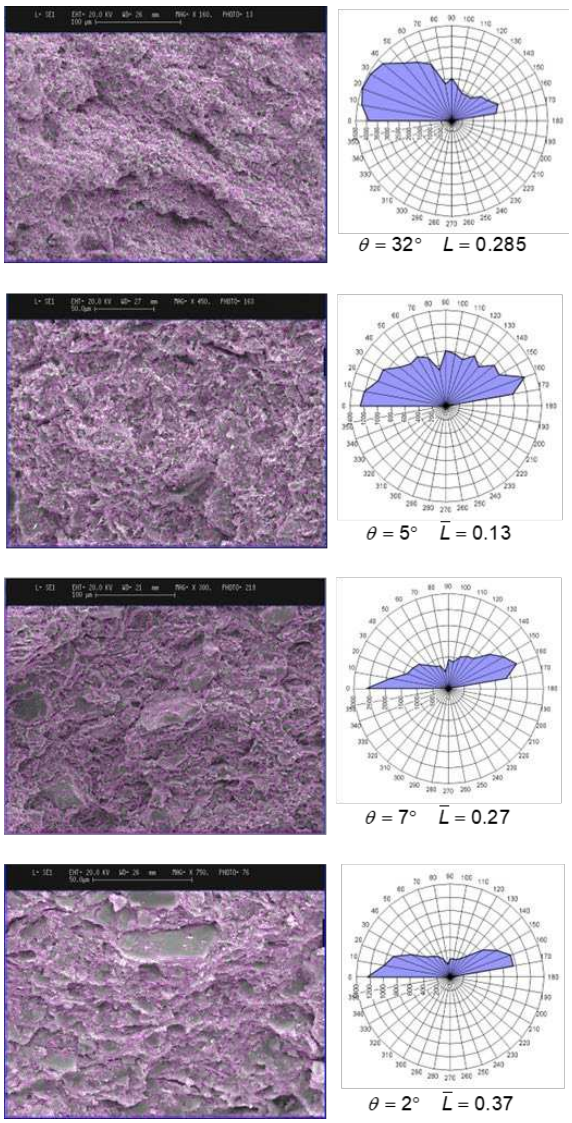

Figure 5,a-d. SEM segmented pictures and directional histograms. Top to bottom, after: consolidometer stage, test 2, test 3 and test 4

4 THERMODYNAMICS WITH INTERNAL VARIALBLES AND ITS APPLICATION TO CLAYS

Thermodynamics with internal variables (in the following TIV) is a framework used to describe the behaviour of complex materials by considering additional state variables that account for their internal structure and history. It tracks back to the pioneering work of Coleman and Gurtin (1967) and Rice (1971), as summarised in Maugin (2015). In this approach, the internal variables can represent various aspects of the material such as microstructural features, damage accumulation, or deformation history, and they are treated as evolving quantities that are linked to the thermodynamic state variables through a set of evolution equations (Maugin, 1992).

The use of internal variables allows the modelling of complex material behaviour beyond the traditional

framework of classical thermodynamics, which assumes that materials are in a state of local equilibrium and are characterized by a fixed set of thermodynamic state variables. By incorporating additional internal variables that describe the evolution of the material's internal structure or history, TIV can provide a more accurate description of materials that exhibit complex behaviour such as viscoelasticity, plasticity, or damage.

TIV has a wide range of applications in materials science, engineering, and physics, and it is used to model a variety of phenomena including fracture, fatigue, creep, and phase transformations. The framework is also useful for developing constitutive models for materials that undergo large deformations, exhibit hysteresis, or display nonlinear responses (e.g. Maugin and Muschik, 1994).

The principles of thermodynamics with internal variables have been successfully adopted to formulate constitutive laws for geomaterials (e.g. Collins and Houlsby, 1997; Einav, 2007; Houlsby, 1981, Houlsby and Puzrin, 2006; Nguyen and Einav, 2009; Rollo and Amorosi, 2020). Most of the above cited research works were developed in what is nowadays called hyperplasticity, that is a framework related to TIV. Fewer contributions to the geomechanics literature can be considered more strictly consistent to TIV, as developed within a rigorous convex analysis mathematical setting (e.g. De Simone and Tamagnini, 2004; Hjiaj and de Saxcé, 2008; Houlsby and Puzrin, 2006; Houlsby, 2019; Marigo and Kazymyrenko, 2019; Nguyen, 2003; Zouain et al., 2007, 2010).

In the following, the general framework of TIV for clays is first briefly outlined, to then focus on the strategies to select the relevant internal variables and the potential functions, all inspired by the micro and macro features of clayey soils discussed in the previous sections. Two examples of the use of the approach to extend well-known hardening plasticity models for clays are finally proposed.

4.1 The general framework

The TIV framework is only briefly summarised below. For a more detailed introduction please refer to the above quoted references.

Within TIV the constitutive behaviour is entirely defined by two potentials: the Helmholtz free energy φ function and the (rate of) dissipation function $\dot{d}$. Limiting the following discussion to rate-independent materials under isothermal conditions and assuming the additive decomposition:

$$\boldsymbol{\varepsilon}^e = \boldsymbol{\varepsilon} - \boldsymbol{\varepsilon}^p \tag{5}$$

the energy function will depend on the current elastic strain state $\boldsymbol{\varepsilon}^e$ and on a set of internal variables $\boldsymbol{\alpha}$ that, for clays can be defined as:

$$\{\boldsymbol{\alpha}\} = \{v, \boldsymbol{\beta}\} \tag{6}$$

where v is the specific volume of the material and $\boldsymbol{\beta}$ is a second order fabric tensor accounting for the orientation distribution of its particles or aggregates. The energy function takes the form:

$$\varphi\left(\boldsymbol{\varepsilon}^e, \boldsymbol{\alpha}\right) = \varphi\left(\boldsymbol{\varepsilon}^e, v, \boldsymbol{\beta}\right) = \varphi\left(\boldsymbol{\varepsilon} - \boldsymbol{\varepsilon}^p, v, \boldsymbol{\beta}\right) \tag{7}$$

It is assumed to be convex and differentiable in v and $\boldsymbol{\beta}$ and strictly convex in $\boldsymbol{\varepsilon}^e$. Taking its partial derivative with respect to the variables it results:

$$\boldsymbol{\sigma} = \frac{\partial \varphi}{\partial \boldsymbol{\varepsilon}^e}; \quad \overline{\chi}_v = -\frac{\partial \varphi}{\partial v}; \quad \overline{\boldsymbol{\chi}}_{\boldsymbol{\beta}} = -\frac{\partial \varphi}{\partial \boldsymbol{\beta}} \tag{8a,b,c}$$

in which $\boldsymbol{\sigma}$ is the Cauchy effective stress tensor, $\overline{\chi}_v$ and $\overline{\boldsymbol{\chi}}_{\boldsymbol{\beta}}$ are the generalised stresses respectively associated to v and $\boldsymbol{\beta}$, and:

$$\overline{\boldsymbol{\chi}}_{\boldsymbol{\varepsilon}^p} = -\frac{\partial \varphi}{\partial \boldsymbol{\varepsilon}^p} = \frac{\partial \varphi}{\partial \boldsymbol{\varepsilon}^e} = \boldsymbol{\sigma} \tag{9}$$

is the generalised stress associated to the plastic strain tensor, here equal to $\boldsymbol{\sigma}$.

The first and second principles of thermodynamics for isothermal processes can be expressed in the form:

$$\dot{\varphi} + \dot{d} = \boldsymbol{\sigma} : \dot{\boldsymbol{\varepsilon}}, \quad \dot{d} \geq 0 \tag{10}$$

where the first is known as the free energy balance equation, equating the rate of the mechanical work to that of the energy and dissipation functions, this latter being always larger of equal to 0.

The rate of the Helmholtz free energy function is:

$$\dot{\varphi}\left(\boldsymbol{\varepsilon}^e, v, \boldsymbol{\beta}\right) = \frac{\partial \varphi}{\partial \boldsymbol{\varepsilon}^e} : \dot{\boldsymbol{\varepsilon}}^e + \frac{\partial \varphi}{\partial v}\dot{v} + \frac{\partial \varphi}{\partial \boldsymbol{\beta}} : \dot{\boldsymbol{\beta}} \tag{11}$$

which combined to Equations (5) and (10) leads to:

$$\left[\frac{\partial \varphi}{\partial \boldsymbol{\varepsilon}^e} - \boldsymbol{\sigma}\right] : \dot{\boldsymbol{\varepsilon}}^e - \boldsymbol{\sigma} : \dot{\boldsymbol{\varepsilon}}^p + \frac{\partial \varphi}{\partial v}\dot{v} + \frac{\partial \varphi}{\partial \boldsymbol{\beta}} : \dot{\boldsymbol{\beta}} + \dot{d} = 0 \tag{12}$$

that holding also in absence of dissipative phenomena (i.e. $\dot{\boldsymbol{\varepsilon}}^p, \dot{v}, \dot{\boldsymbol{\beta}}, \dot{d}$ all equal to 0) confirms the state Equation (8a). As such, the rate of dissipation takes the form:

$$\dot{d} = \dot{d}\left(\boldsymbol{\sigma}, v, \boldsymbol{\beta}, \dot{\boldsymbol{\varepsilon}}^p, \dot{v}, \dot{\boldsymbol{\beta}}\right) = \boldsymbol{\sigma} : \dot{\boldsymbol{\varepsilon}}^p + \overline{\chi}_v \dot{v} + \overline{\boldsymbol{\chi}}_{\boldsymbol{\beta}} : \dot{\boldsymbol{\beta}} \geq 0 \quad (13)$$

For a rate independent material the dissipation function is first order homogeneous in the rate of $\boldsymbol{\varepsilon}^p$, v and $\boldsymbol{\beta}$. Consequently, according to the Euler's theorem, in the ideal case of a differentiable rate of dissipation it follows:

$$\dot{d} = \frac{\partial \dot{d}}{\partial \dot{\boldsymbol{\varepsilon}}^p} : \dot{\boldsymbol{\varepsilon}}^p + \frac{\partial \dot{d}}{\partial v}\dot{v} + \frac{\partial \dot{d}}{\partial \dot{\boldsymbol{\beta}}} : \dot{\boldsymbol{\beta}} \geq 0 \quad (14)$$

where $\boldsymbol{\chi}_{\boldsymbol{\varepsilon}^p} = \partial \dot{d} / \partial \dot{\boldsymbol{\varepsilon}}^p$, $\chi_v = \partial \dot{d} / \partial \dot{v}$ and $\boldsymbol{\chi}_{\boldsymbol{\beta}} = \partial \dot{d} / \partial \dot{\boldsymbol{\beta}}$ are called dissipative generalised stress that, according to the orthogonality principle (Ziegler, 1977), are here assumed equal to the corresponding generalised stresses:

$$\boldsymbol{\chi}_{\boldsymbol{\varepsilon}^p} = \boldsymbol{\sigma}, \quad \chi_v = \overline{\chi}_v, \quad \boldsymbol{\chi}_{\boldsymbol{\beta}} = \overline{\boldsymbol{\chi}}_{\boldsymbol{\beta}} \quad (15)$$

An element of complexity that characterises the application of TIV in the context of the material models discussed here is that they require non-differentiable rate of dissipations to reproduce the expected mechanical behaviour. For example, the rate of dissipation, which is first order homogeneous in $\dot{\boldsymbol{\varepsilon}}^p, \dot{v}$ and $\dot{\boldsymbol{\beta}}$, is not differentiable when these variables are all equal to zero. As such, instead of the above partial derivatives, the following more rigorous convex analysis-based definitions of the dissipative generalised stresses should be used:

$$\boldsymbol{\chi}_{\boldsymbol{\varepsilon}^p} \in \partial_{\dot{\boldsymbol{\varepsilon}}^p} \dot{d} \; ; \; \boldsymbol{\chi}_v \in \partial_{\dot{v}} \dot{d} \; ; \; \boldsymbol{\chi}_{\boldsymbol{\beta}} \in \partial_{\dot{\boldsymbol{\beta}}} \dot{d} \quad (16)$$

in which the subgradients on the left side of the relationships define the sets each generalised dissipative stress belongs to (as indicated by the symbol $\in$), thus overpassing the limitation related to the non-differentiability of the rate of dissipation potential.

Again, relaying on convex analysis tools, it is possible to switch from the rate of dissipation function to the corresponding yield domain that constrains the admissible states in the generalised stress space:

$$\mathsf{K} = \left\{ \left\{ \boldsymbol{\sigma}, v, \boldsymbol{\beta}, \boldsymbol{\chi}_{\boldsymbol{\varepsilon}^p}, \chi_v, \boldsymbol{\chi}_{\boldsymbol{\beta}} \right\} \middle| \, \overline{f}\left(\boldsymbol{\sigma}, v, \boldsymbol{\beta}, \boldsymbol{\chi}_{\boldsymbol{\varepsilon}^p}, \chi_v, \boldsymbol{\chi}_{\boldsymbol{\beta}}\right) \leq 0 \right\} \quad (17)$$

by obtaining its indicator function:

$$I_{\mathsf{K}} := \begin{cases} = 0, \text{ if } \left\{ \boldsymbol{\sigma}, v, \boldsymbol{\beta}, \boldsymbol{\chi}_{\boldsymbol{\varepsilon}^p}, \chi_v, \boldsymbol{\chi}_{\boldsymbol{\beta}} \right\} \in \mathsf{K} \\ + \infty, \text{ otherwise} \end{cases} \quad (18)$$

solving the following Legendre-Fenchel transform:

$$I_{\mathsf{K}} = \sup_{\left(\dot{\boldsymbol{\varepsilon}}^p, \dot{v}, \dot{\boldsymbol{\beta}}\right)} \left\{ \boldsymbol{\chi}_{\boldsymbol{\varepsilon}^p} : \dot{\boldsymbol{\varepsilon}}^p + \chi_v \dot{v} + \boldsymbol{\chi}_{\boldsymbol{\beta}} : \dot{\boldsymbol{\beta}} - \dot{d}\left(\boldsymbol{\sigma}, v, \boldsymbol{\beta}, \dot{\boldsymbol{\varepsilon}}^p, \dot{v}, \dot{\boldsymbol{\beta}}\right) \right\} \quad (19)$$

in which $\boldsymbol{\sigma}, v, \boldsymbol{\beta}$ play the role of passive variables in the search for the least upper bound of the set in braces operated by the supremum (sup).

A key result of convex analysis (see for example Han and Reddy, 1999) is the normality rule that holds in the generalised stress space, leading to evolution laws for the internal variables that, in the case of a differentiable function $\overline{f}$, result as:

$$\dot{\boldsymbol{\varepsilon}}^p = \dot{\gamma} \frac{\partial \overline{f}}{\partial \boldsymbol{\chi}_{\boldsymbol{\varepsilon}^p}}$$
$$\dot{v} = \dot{\gamma} \frac{\partial \overline{f}}{\partial \chi_v} \quad (20a,b,c)$$
$$\dot{\boldsymbol{\beta}} = \dot{\gamma} \frac{\partial \overline{f}}{\partial \boldsymbol{\chi}_{\boldsymbol{\beta}}}$$

in which $\dot{\gamma} \geq 0$ is the plastic multiplier of the classical plasticity theory.

As a final step, it is worth establishing the corresponding yield criterion in the Cauchy stress space, expressing $\overline{f}$ as a function of $\boldsymbol{\sigma}, v, \boldsymbol{\beta}$ via Equations (15) and (8), obtaining the more familiar:

$$f\left(\boldsymbol{\sigma}, v, \boldsymbol{\beta}\right) \leq 0 \quad (21)$$

At this stage the whole structure of a single surface hardening plasticity model is recovered, though derived within a more general theoretical setting. This latter offers the advantage of ensuring that the formulation meets the principles of thermodynamics and, at the same time, consistently accounts for the possibly more comprehensive couplings between different aspects of the mechanics of the studied material, as will be briefly illustrated in the two final examples of this section.

4.2 Micro-inspired selection of internal variables and potential functions

As previously anticipated, internal variables are meant to represent the average microstructural features that control the macroscopic mechanical behaviour of the material. By definition, internal variables should in principle be measurables while not being controllable: their evolution is driven by energy dissipation, as represented in Equation (14) in which at each internal variable corresponds a generalised stress acting on its rate. The number of internal variables should be kept as small as possible but sufficient to describe the key features of the material.

In light of what discussed in Section 2, in the case of reconstituted or soft clays a first attempt to describe their mechanical behaviour should involve, as internal variables, the inter-aggregates porosity, or any equivalent scalar as the specific volume v, a tensor-valued fabric descriptor, as the second order symmetric tensor $\boldsymbol{\beta}$ accounting for the orientation distribution of the aggregates, and the plastic strain tensor $\boldsymbol{\varepsilon}^p$, to describe the frictional behaviour stemming from the mutual interacions between aggregates of particles. This latter variable will only enter the formulation by its rate, to avoid the conceptual limitation related to the impossibility of performing a direct measurement of the plastic strain cumulated by a natural material in its geological history, along the line of what discussed in Rubin (2001).

In detail, specific volume and its rate are defined as:

$$v = \frac{V}{V_s}; \quad \frac{\dot{v}}{v} = \frac{\dot{V}}{V} - \frac{\dot{V}_s}{V_s} \tag{22}$$

where V is the total volume and V_s the volume of the solids. Recalling the definition of the total volumetric strain rate ($\dot{\varepsilon}_v = -\dot{V}/V$), assuming the additive decomposition of elastic and plastic strains and, according to Collins et al. (2010), identifying the elastic volumetric strain rate as the variation of the solids volume, it results:

$$\dot{\varepsilon}_v^e = -\frac{\dot{V}_s}{V_s} \quad ; \quad \dot{\varepsilon}_v^p = -\frac{\dot{v}}{v} \tag{23a,b}$$

This assumption, originally proposed for granular materials, can also be adopted, as a first approximation, for clays, based on the hypothesis that aggregates of particles mainly deform elastically as for example discussed in Pedrotti and Tarantino (2018). Equation (23) implies that the specific volume can be adopted as suitable internal variable within the thermodynamic constitutive framework to describe the dissipative processes involved in permanent modifications of the porosity in clays. It is worth noting that, differently from Rollo and Amorosi (2022), here the specific volume is adopted instead of the preconsolidation pressure p_c. Nonetheless, the two variables can be related by:

$$\dot{p}_c = -\frac{p_c}{\lambda^*}\frac{\dot{v}}{v} \quad ; \quad p_c = p_r\left(\frac{v}{N}\right)^{-\frac{1}{\lambda^*}} \tag{24a,b}$$

where N is the specific volume at the reference pressure p_r and λ^* the parameter governing the isotropic hardening law in the Cam Clay-family plasticity models.

The other internal variable $\boldsymbol{\beta}$ is a second order fabric tensor accounting for the orientation distribution of the aggregates. In the following, its evolution is assumed to be related to plastic strain rates, according to the distortional hardening law proposed by Rollo and Amorosi (2022):

$$\dot{\boldsymbol{\beta}} = c\left(\boldsymbol{\beta}_b - \boldsymbol{\beta}\right)\sqrt{\left(\dot{\varepsilon}_v^p + \boldsymbol{\beta} : \dot{\boldsymbol{\varepsilon}}'^p\right)^2 + \frac{2}{3}\left(M^2 - \beta^2\right)\dot{\boldsymbol{\varepsilon}}'^p : \dot{\boldsymbol{\varepsilon}}'^p} \tag{25}$$

where M is the stress ratio at critical state and $\boldsymbol{\varepsilon}'^p$ the deviatoric plastic strain tensor. β is the triaxial counterpart of $\boldsymbol{\beta}$, $\beta = \sqrt{3/2\,\boldsymbol{\beta} : \boldsymbol{\beta}}$, c is a parameter controlling the pace of the evolution and $\boldsymbol{\beta}_b$ represents the equilibrium "bounding" value towards which $\boldsymbol{\beta}$ tends to, function of the current stress ratio $\mathbf{r} = \mathbf{s}/p$, with $\mathbf{s}$ deviatoric part of the effective stress, for which different expression have been provided in the literature (e.g. Dafalias and Taiebat, 2013).

The selection of the energy function is pursued by analysing the experimental observations of wave propagations carried out at different states of the material. In detail, the starting point of the process is that of assuming for the energy function the general expression of Equation (7), such that:

$$\boldsymbol{\sigma} = \frac{\partial \varphi\left(\boldsymbol{\varepsilon}^e, v, \boldsymbol{\beta}\right)}{\partial \boldsymbol{\varepsilon}^e} \tag{26}$$

and, after differentiation:

$$\dot{\boldsymbol{\sigma}} = \frac{\partial^2 \varphi\left(\boldsymbol{\varepsilon}^e, v, \boldsymbol{\beta}\right)}{\partial \boldsymbol{\varepsilon}^e \otimes \partial \boldsymbol{\varepsilon}^e}\dot{\boldsymbol{\varepsilon}}^e + \frac{\partial^2 \varphi\left(\boldsymbol{\varepsilon}^e, v, \boldsymbol{\beta}\right)}{\partial \boldsymbol{\varepsilon}^e \partial v}\dot{v} + \frac{\partial^2 \varphi\left(\boldsymbol{\varepsilon}^e, v, \boldsymbol{\beta}\right)}{\partial \boldsymbol{\varepsilon}^e \otimes \partial \boldsymbol{\beta}}\dot{\boldsymbol{\beta}} \tag{27}$$

The first term on the right side of Equation (27) is the fourth order reversible stiffness tensor, which is the only one detected during wave propagation tests, as the perturbations induced in the soil are small enough not to determine any instantaneous variation of the specific volume ($\dot{v} = 0$) and of the fabric tensor ($\dot{\boldsymbol{\beta}} = 0$). As such, this can be interpreted as an instantaneous picture of the response of the soil, depending on the energy content via its current state, i.e. $\boldsymbol{\varepsilon}^e$, or its dual $\boldsymbol{\sigma}$, v and $\boldsymbol{\beta}$. In the laboratory experiments discussed in Section 3, wave propagation tests were carried out at different states, providing a comprehensive data set, sufficient to back-evaluate an analytical expression for the energy function of Equation (7), as discussed in Houlsby et al. (2005, 2019) and in Amorosi et al. (2020).

For what concerns the selection of the dissipation function, the following assumptions have been adopted.

First of all, the function has to be homogeneous of degree one in the rates $\dot{\boldsymbol{\varepsilon}}^p$, $\dot{v}$ and $\dot{\boldsymbol{\beta}}$, aiming at considering a rate-independent behaviour. Furthermore, it has to be strictly positive for non-zero values of the above rates and equal to zero in the absence of such rates. The structure of the rate of dissipation functions adopted in the following examples is inspired by the pioneering work of Houlsby (1981) and its extension discussed in Collins and Houlsby (1997), in which for a Cam-Clay family model the following function was proposed:

$$\dot{d}\left(\dot{\varepsilon}_v^p, \dot{\varepsilon}_s^p, p_c\right) = \frac{p_c}{2}\left(\sqrt{\dot{\varepsilon}_v^{p2} + M^2\dot{\varepsilon}_s^{p2}} + \dot{\varepsilon}_v^p\right) \qquad (28)$$

where the square root term, an Euclidean norm of the volumetric and weighted deviatoric plastic strain rates, is scaled by half of the preconsolidation pressure p_c. This leads to a pseudo-frictional material whose dissipative response does not depend on the mean effective pressure, as customary in coarse-grained soils, but on p_c, here tracking the permanent evolution of the porosity of the clay. The last term in the expression provides a shift of the resulting yield domain in the generalised stress space: it represents an alternative option as compared to the one originally proposed by Houlsby (1981), where such a term is absent in the dissipation function but appears, once integrated in time, as an additional term in the energy function. A general discussion on the implications of the above two alternative options is out of the scope of this paper: the interested reader can refer to Gurtin and Reddy (2009) and to the more recent Ulloa et al. (2021) for further details.

The dissipation functions adopted in the following examples origin from Equation (28), introducing the necessary specific modifications that are commented in detail in the following.

4.3 Example 1: a revised Modified Cam-Clay model

This first example consists of an updated version of the well-known Modified Cam-Clay model, in which the key mechanical modifications are inspired by some of the experimental results discussed in Sections 2 and 3. Here the specific volume is assumed as the internal variable tracking the past history of the material: it appears explicitly in the energy function, such that this latter not only accounts for the non-linear dependence of the stiffness on the current stress (or elastic strain) state, following Houlsby et al. (2005), but also depends on the current specific volume, resulting in:

$$\varphi\left(\varepsilon_v^e, \varepsilon_s^e, v\right) = \left(\frac{v}{N}\right)^{\frac{r}{(n-1)\lambda^*}} \left\{\frac{p_r}{k(2-n)} k^{\frac{2-n}{1-n}} (1-n)^{\frac{2-n}{1-n}} \left[\varepsilon_v^{e2} + \frac{3g}{k(1-n)}\varepsilon_s^{e2}\right]^{\frac{2-n}{2-2n}}\right\} \qquad (29)$$

in which n, k and g are the parameters of the hyperelastic potential of Houlsby et al. (2005), here in braces, scaled by the specific volume function via the parameter r. All these parameters can be easily calibrated based on shear wave propagation experiments.

For what concerns the rate of dissipation the following expression is here adopted:

$$\dot{d}\left(\dot{\varepsilon}_v^p, \dot{\varepsilon}_s^p, \dot{v}, v\right) = \frac{p_r}{2}\left(\frac{v}{N}\right)^{-\frac{1}{\lambda^*}} \left(\sqrt{\dot{\varepsilon}_v^{p2} + M^2\dot{\varepsilon}_s^{p2}} + \dot{\varepsilon}_v^p\right) + I_K\left(\frac{\dot{v}}{v} + \dot{\varepsilon}_v^p\right) \qquad (30)$$

in which the preconsolidation pressure of Equation (28) is substituted by its specific volume counterpart based on Equation (24b). Furthermore, the last term is an indicator function imposing as a constraint the fundamental assumption of Equation (23b) such that:

$$I_{K[0,0]} := \begin{cases} = 0, \text{ if } \left(\frac{\dot{v}}{v} + \dot{\varepsilon}_v^p\right) \in K \rightarrow -\frac{\dot{v}}{v} = \dot{\varepsilon}_v^p \\ + \infty, \text{otherwise} \end{cases} \qquad (31)$$

By standard application of the convex analysis-based procedure previously illustrated, the above rate of dissipation leads to the following yield domain in the generalised stress space:

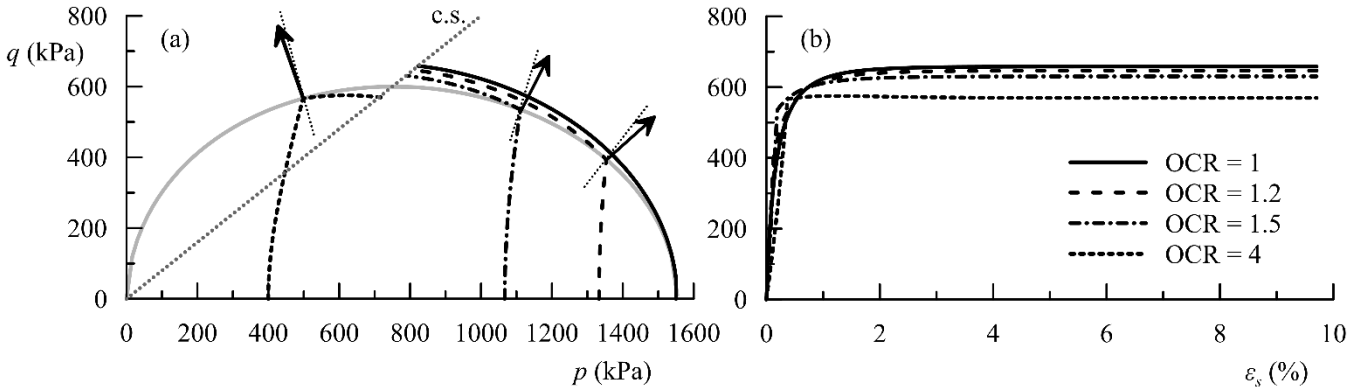

Figure 6. Revised Modified Cam-Clay model: initial yield domain and stress paths (left); stress-strain response (right)

$$\bar{f} = \chi_q^2 + M^2\left(\chi_p - v\chi_v\right)\left[\chi_p - v\chi_v - p_r\left(\frac{v}{N}\right)^{-\frac{1}{\lambda^*}}\right] \leq 0 \quad (32)$$

and to the corresponding yield domain f in the Cauchy stress space, represented in Figure 6.

One of the key features of this isotropic formulation is the intrinsic coupling of the energy and dissipation functions, both dependent on the internal variable v. This not only implies the dependence of the reversible behaviour on the previously experienced irreversible history, tracked by the specific volume, but also makes the irreversible behaviour affected by the above coupling, resulting in a non-associated flow response in the Cauchy stress space. This is illustrated in Figure 6 with reference to four triaxial undrained simulations carried out at different overconsolidation ratios, whose stress-strain curves are also shown in the figure. Tests were carried out with reference to the parameters indicated in black in Table 1.

Table 1. Model parameters

Parameter	Value	Parameter	Value
p_r (kPa)	100	M	1.0
n	0.8	λ^*	0.07
k	67	c	30
g	50	z	2.5
r	0.4	s	5.0
N	1.8	ω	1.5

4.4 Example 2: a revised Saniclay model

In this section a TIV-based anisotropic model for clays is outlined. It can be considered as an extension of the formulations proposed by Dafalias et al. (2006) and by Dafalias and Taiebat (2013), all belonging to the family of simple anisotropic clay plasticity models (Saniclay).

Here both the specific volume and the fabric tensor are assumed as internal variables tracking the past history of the material: they appear explicitly in the energy function, such that this latter accounts for the non-linear dependence of the stiffness on the current effective stress (or elastic strain) state, following Houlsby et al. (2019) and Amorosi et al. (2020). It also depends on the current values of the specific volume and fabric tensor, resulting in:

$$\varphi\left(\boldsymbol{\varepsilon}^e, v, \boldsymbol{\beta}\right) = \left(\frac{v}{N}\right)^{\frac{r}{(n-1)\lambda^*}} \frac{p_r}{k\left(2-n\right)} k^{\frac{2-n}{1-n}} \left(1-n\right)^{\frac{2-n}{1-n}} \left\{\left[k\left(1-n\right) - \frac{2}{3}g\right]\mathrm{tr}^2\left(\boldsymbol{\varepsilon}^e - \omega\beta\boldsymbol{\beta}\boldsymbol{\varepsilon}^e\right) + 2g\,\mathrm{tr}\left[\left(\boldsymbol{\varepsilon}^e - \omega\beta\boldsymbol{\beta}\boldsymbol{\varepsilon}^e\right)^2\right]\right\}^{\frac{2-n}{2-2n}} \quad (33)$$

where ω is an additional model parameter controlling the intrinsic attitude of the clay to develop anisotropy, which can be estimated as a function of its plasticity index (Amorosi et al., 2021).

The dissipation function proposed for this model is the following:

$$\dot{d}\left(v, \boldsymbol{\beta}, \dot{\boldsymbol{\varepsilon}}^p, \dot{v}, \dot{\boldsymbol{\beta}}\right) = \frac{p_r}{2}\left(\frac{v}{N}\right)^{-\frac{1}{\lambda^*}}\left(\dot{\bar{d}} + \dot{\varepsilon}_v^p + \boldsymbol{\beta}:\dot{\boldsymbol{\varepsilon}}'^p\right) + I_K\left(\frac{\dot{v}}{v} + \dot{\varepsilon}_v^p\right) + I_L\left[\dot{\boldsymbol{\beta}} - c\left(\boldsymbol{\beta}_b - \boldsymbol{\beta}\right)\dot{\bar{d}}\right] \quad (34)$$

with:

$$\dot{\bar{d}} = \sqrt{\left(\dot{\varepsilon}_v^p + \boldsymbol{\beta}:\dot{\boldsymbol{\varepsilon}}'^p\right)^2 + \frac{2}{3}\left(M^2 - \beta^2\right)\dot{\boldsymbol{\varepsilon}}'^p:\dot{\boldsymbol{\varepsilon}}'^p} \quad (35)$$

and:

$$I_{L[0,0]} := \begin{cases} = 0, \text{ if } \left[\dot{\boldsymbol{\beta}} - c\left(\boldsymbol{\beta}_b - \boldsymbol{\beta}\right)\dot{\bar{d}}\right] \in L \rightarrow \dot{\boldsymbol{\beta}} = c\left(\boldsymbol{\beta}_b - \boldsymbol{\beta}\right)\dot{\bar{d}} \\ +\infty, \text{ otherwise} \end{cases} \quad (36)$$

Comparing Equations (30) to (34) it clearly emerges that the former is formulated in terms of direct invari-

ants of the rate of plastic strain, given the isotropic character of the model, while this is not possible for the latter, as aimed at accounting for anisotropy. Furthermore, in the proposed anisotropic rate of dissipation the term $\dot{\tilde{d}}$ is again an Euclidean norm now explicitly dependent on the fabric tensor $\boldsymbol{\beta}$, leading to distorted yield domain in the generalised stress space and, consequently, in the Cauchy one. Finally, the two indicator functions I_K and I_L act as constraints to ensure that Equations (23) and (25) are satisfied in the irreversible regime.

A series of tests have been simulated to highlight some of the features of this extended Saniclay model, all based on the parameters reported in Table 1, now including also those indicated in blue. In all the test simulations the following expression for $\boldsymbol{\beta}_b$ was adopted (Dafalias and Taiebat, 2013):

$$\boldsymbol{\beta}_b = \sqrt{\frac{2}{3}}\frac{M}{z}\left[1-\exp\left(-s\frac{|\eta|}{M}\right)\right]\frac{\mathbf{r}}{\|\mathbf{r}\|} \tag{37}$$

in which:

$$\mathbf{r} = \frac{\mathbf{s}}{p};\quad \|\mathbf{r}\| = \sqrt{\mathbf{r}:\mathbf{r}};\quad |\eta| = \sqrt{\frac{3}{2}\mathbf{r}:\mathbf{r}} \tag{38}$$

leading to a non-linear dependence of $\boldsymbol{\beta}_b$ on the current direction of the stress path as expressed by its generalised stress ratio. Figure 7 illustrates the results of two constant radial triaxial stress path tests, respectively characterised by η equal to 0 (isotropic) and 0.6, applied to the same initially isotropic clay, characterised by p = 200 kPa and v = 1.633. The model predicts a different evolution of the yield surface, which in both cases expands due to the reduction of the specific volume, while keeping centred in the case of the isotropic path or experiencing a substantial distortion in the η = 0.6 case. This is related to the different evolution of the fabric tensor $\boldsymbol{\beta}$ in the two tests, which reflects into the corresponding different evolution of the stiffness anisotropy ratio, also shown in Figure 7. Those patters resemble what observed by Mitaritonna et al. (2014), as discussed in Section 3. Finally, a series of undrained triaxial tests were simulated after imposing a virgin radial loading along the η = 0.6 stress path followed, in two cases, by a radial unloading prior to shearing. The results are illustrated in Figure 8 in terms of undrained stress paths, stress-strain curves, and evolution of the stiffness anisotropy ratio: it results that during the simulated shearing stages the clay does not experience significant fabric evolution, as confirmed by the minor modifications observed in terms of stiffness anisotropy ratio.

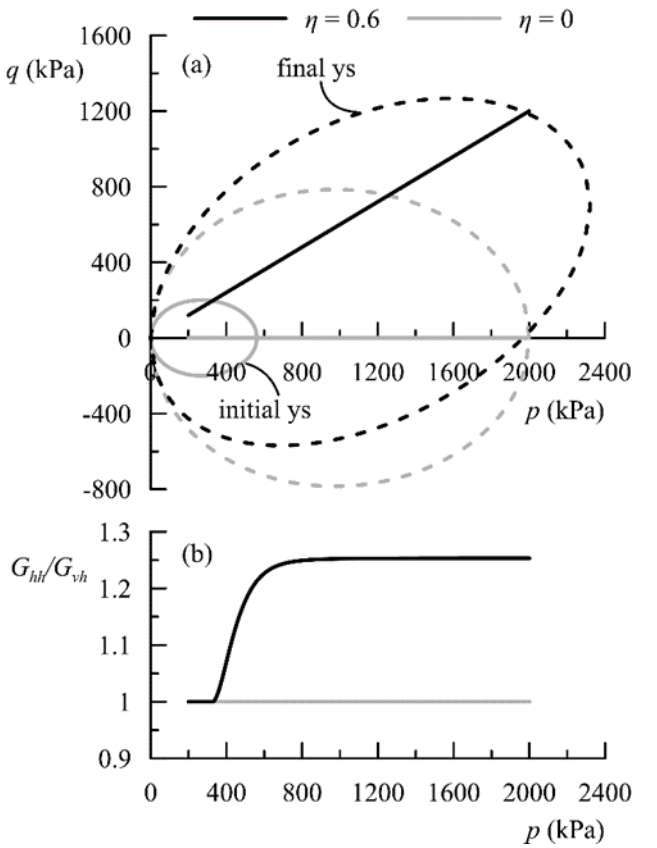

Figure 7. Radial stress paths and related evolution of the stiffness anisotropy ratio

5 CONCLUSIONS AND FUTURE DEVELOPMENTS

Clays are ubiquitous in geotechnical and environmental engineering applications and understanding their complex mechanical behaviour is essential for designing and constructing safe and efficient structures.

Over the years, numerous constitutive models have been developed to describe their mechanical behaviour, but only few of them were formulated in light of the complex microstructural features of these materials.

Recently, there has been a growing interest in micro-inspired constitutive modelling of clays, which seeks to incorporate microscale processes and properties into macroscopic constitutive models. This approach involves understanding the micromechanical behaviour of clays, including the role of particle/aggregate porosity and fabric evolution, using this knowledge to develop macroscopic models that capture the behaviour of these materials. Micro-inspired constitutive modelling has the potential to improve the accuracy and reliability of constitutive models for clays and ultimately lead to safer and more efficient geotechnical and environmental engineering practices.

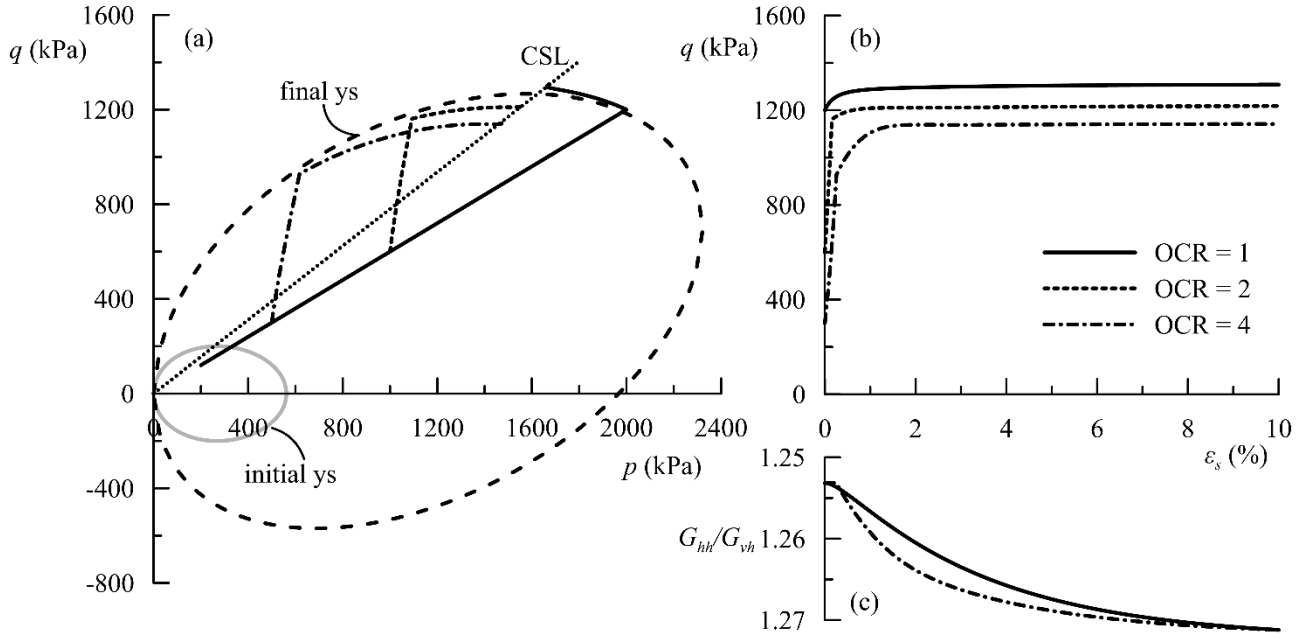

Figure 8. Revised Saniclay model: initial yield domain and stress paths (left); stress-strain response and evolution of the elastic stiffness anisotropy ratio (right)

The aim of this paper was that of providing an overview of some recent advances in micro-inspired constitutive modelling of clays. After a review of multi-scale experimental evidences and their possible interpretation and generalisation in terms of internal variables controlling the mechanics of clayey soils, two examples of constitutive models were proposed, both developed in the framework of Thermodynamics with Internal Variables. This theoretical environment proves to effectively allow the development of constitutive models that not only respect the fundamental principles of thermodynamics, but also directly benefit from our understanding of the complex micromechanics of clayey soils.

The ongoing development of new and more accurate experimental tools, providing quantitative insights into the micromechanics of clays, together with the parallel development of DEM-based numerical models, specifically formulated for these complex materials (e.g. Pagano et al., 2020), represent a promising context for the development of future research, aimed at bridging the gap between the micro- and macro-scale in clay soils.

6 ACKNOWLEDGEMENTS

The author acknowledges the support by the research project RETURN - multi-Risk sciEnce for resilienT commUnities undeR a changiNg climate - funded by the European Union within the Italian Recovery and Resilience Plan (PNRR). He also wants to thank Dr. Fabio Rollo for the scientific support in the development of the work summarised in this paper, and Dr. Marialuigia Sangirardi for the critical review of the manuscript.

7 REFERENCES

Amorosi, A., Rollo, F., Dafalias, Y.F. 2021. Relating elastic and plastic fabric anisotropy of clays, *Géotechnique* **71**(7), 583-593.

Amorosi, A., Rollo, F., Houlsby, G. T. 2020. A nonlinear anisotropic hyperelastic formulation for granular materials: comparison with existing models and validation. *Acta Geotechnica*, **15**, 179-196.

Anandarajah, A. 2000a. Numerical simulation of one-dimensional behavior of a kaolinite, *Géotechnique* **50**(5), 509–519.

Anandarajah, A., 2000b. On influence of fabric anisotropy on the stress–strain behavior of clays, *Computers and Geotechnics* **27**, 1–17.

Barden, L., Sides, G. R. 1970. Engineering behavior and structure of compacted clay. *Journal of the Soil Mechanics and Foundations Division* **96(**4), 1171–1200.

Callisto, L., Calabresi, G. 1998. Mechanical behaviour of a natural soft clay, *Géotechnique* **48**(4), 495-513.

Cetin, H. 2004. Soil-particle and pore orientations during consolidation of cohesive soils, *Engineering geology* **73**(1-2), 1-11.

Chang, C. S., Hicher, P. Y., Yin, Z. Y., Kong, L. R. 2009. Elastoplastic model for clay with microstructural consideration, *Journal of engineering mechanics* **135**(9), 917-931.

Chow, J. K., Li, Z., Wang, Y. H. 2019. Comprehensive microstructural characterizations of 1-D consolidated kaolinite samples with fabric tensors and pore elongation factors, *Engineering Geology* **248**, 22-33.

Coleman, B.D, Gurtin, M.E. 1967. Thermodynamics with internal state variables, *J.Chem. Phys.* **47**, 597–613.

Collins, I. F., Houlsby, G. T. 1997. Application of thermomechanical principles to the modelling of geotechnical ma-

terials. *Proceedings of the Royal Society of London. Series A: Mathematical, Physical and Engineering Sciences*, **453**, 1975-2001.

Collins, I. F., Muhunthan, B., Qu, B. 2010. Thermomechanical state parameter models for sands. *Géotechnique*, **60**(8), 611-622.

Cotecchia, F., Chandler, R. J. 1998. One-dimensional compression of a natural clay: structural changes and mechanical effects. *The geotechnics of hard soils-soft rocks*: *Proceedings, 2nd International Symposium on Hard Soils - Soft* Rocks,103-114. A. A. Balkema, Rotterdam.

Dafalias, Y. F. 1986. An anisotropic critical state soil plasticity model. *Mechanics research communications* **13**(6), 341-347.

Dafalias, Y. F., Manzari, M. T., Papadimitriou, A. G. 2006. SANICLAY: simple anisotropic clay plasticity model. *International Journal for Numerical and Analytical Methods in Geomechanics*, **30**(12), 1231-1257.

Dafalias, Y. F., Taiebat, M. 2013. Anatomy of rotational hardening in clay plasticity. *Géotechnique*, **63**(16), 1406-1418.

Delage, P., Lefebvre, G. 1984. Study of the structure of a sensitive Champlain clay and of its evolution during consolidation, *Canadian Geotechnical Journal* **21**(1), 21-35.

De Simone, A., Tamagnini, C. 2005. Stress–dilatancy based modelling of granular materials and extensions to soils with crushable grains, *International journal for numerical and analytical methods in geomechanics* **29**(1), 73-101.

Einav, I. 2007. Breakage mechanics—part I: theory, *Journal of the Mechanics and Physics of Solids* **55**(6), 1274-1297.

Fu, P., Dafalias, Y. F. 2015. Relationship between void-and contact normal-based fabric tensors for 2D idealized granular materials *International Journal of Solids and Structures* **63**, 68-81.

Gao, Q. F., Jrad, M., Hattab, M., Fleureau, J. M., Ameur, L. I. 2020. Pore morphology, porosity, and pore size distribution in kaolinitic remolded clays under triaxial loading, *International Journal of Geomechanics* **20**(6), 04020057.

Gens, A. 1982. *Stress–strain and strength characteristics of a low plasticity clay* (PhD thesis), Imperial College, London, UK.

Guglielmi, S., Cotecchia, F., Cafaro, F., Gens, A. 2022. Analysis of the micro to macro response of clays to compression, *Géotechnique*, 1-21.

Gurtin, M. E., Reddy, B. D. 2009. Alternative formulations of isotropic hardening for Mises materials, and associated variational inequalities. *Continuum Mechanics and Thermodynamics*, **21**, 237-250.

Hattab, M., Chang, C. S. 2015. Interaggregate forces and energy potential effect on clay deformation, *Journal of engineering mechanics* **141**(7), 04015014.

Hattab, M., Fleureau, J. M. 2010. Experimental study of kaolin particle orientation mechanism, *Géotechnique* **60**(5), 323-331.

Hattab, M., Hammad, T., Fleureau, J. M., Hicher, P. Y. 2013. Behaviour of a sensitive marine sediment: microstructural investigation, *Géotechnique* **63**(1), 71-84.

Hicher, P. Y., Wahyudi, H., Tessier, D. 2000. Microstructural analysis of inherent and induced anisotropy in clay. *Mechanics of Cohesive-frictional Materials: An International Journal on Experiments, Modelling and Computation of Materials and Structures* **5**(5), 341-371.

Houlsby, G. T. 1981. *Study of plasticity theories and their applicability to soils* (Doctoral dissertation), University of Cambridge, Cambridge, UK.

Houlsby, G. T. 2019. Frictional plasticity in a convex analytical setting, *Open Geomechanics* **1**, 1-10.

Houlsby, G. T., Puzrin, A. M. 2006. *Principles of hyperplasticity: an approach to plasticity theory based on thermodynamic principles*, Springer Verlag, London, UK.

Houlsby, G. T., Amorosi, A., Rojas, E. 2005. Elastic moduli of soils dependent on pressure: a hyperelastic formulation. *Géotechnique*, **55**(5), 383-392.

Houlsby, G. T., Amorosi, A., Rollo, F. 2019. Non-linear anisotropic hyperelasticity for granular materials. *Computers and Geotechnics*, **115**, 103167.

Hueckel, T., Tutumluer, E. 1994. Modeling of elastic anisotropy due to one-dimensional plastic consolidation of clays, *Computer and Geotechnics* **16**(4), 311–349.

Hjiaj, M., de Saxcé, G. 2008. Variational formulation of the Cam-Clay model. *Proceedings, IUTAM Symposium on Theoretical, Computational and Modelling Aspects of Inelastic Media*,165-174. Springer, Netherlands.

Jaky, J. 1944. The coefficient of earth pressure at rest, *Journal of the Society of Hungarian Architects and engineers* **78**(22), 355–358.

Kanatani, K. I. 1984. Stereological determination of structural anisotropy. *International Journal of Engineering Science*, **22**(5), 531-546.

Kavvadas, M. 1983. A constitutive model for clays based on non-associated anisotropic elasto-plasticity. *Proceedings, International Conference on Constitutive Laws for Engineering Materials–Theory and Application*, 10-14.

Kim, T., Finno, R. J. 2012. Anisotropy evolution and irrecoverable deformation in triaxial stress probes, *Journal of Geotechnical and Geoenvironmental Engineering* **138**(2), 155–165.

Lewin, P. I. 1973. The influence of stress history on the plastic potential. *Proceedings, Symposium on the Role of Plasticity in Soil Mechanics,* Cambridge, England. (No. Conf Paper).

Marigo, J. J., Kazymyrenko, K. 2019. A micromechanical inspired model for the coupled to damage elasto-plastic behavior of geomaterials under compression, *Mechanics & Industry* **20**(1), 105.

Martínez-Nistal, A., Veniale, F., Setti, M., Cotecchia, F. 1999. A scanning electron microscopy image processing method for quantifying fabric orientation of clay geomaterials, *Applied Clay Science* **14**(4), 235-243.

Maugin,G.A., Muschik,W. 1994. Thermodynamics with internal variables. I. General Concepts, II. Applications. *Journal of Non-Equilibrium Thermodynamics* **19**, 217-249, 250-289.

Maugin, G. A. 2015. The saga of internal variables of state in continuum thermo-mechanics (1893–2013). *Mechanics Research Communications*, **69**, 79-86.

Mitaritonna, G., Amorosi, A., Cotecchia, F. 2014. Experimental investigation of the evolution of elastic stiffness anisotropy in a clayey soil, *Géotechnique* **64**(6), 463-475.

Mitchell, J. K. 1956. The fabric of natural clays and its relation to engineering properties. *Proceedings of the Thirty-*

Fifth Annual Meeting of the Highway Research Board, 693-713. Highway Research Board.

Nguyen, Q. S. 2003. On shakedown analysis in hardening plasticity, *Journal of the Mechanics and Physics of Solids* **51**(1), 101-125.

Nguyen, G. D., Einav, I. 2009. The energetics of cataclasis based on breakage mechanics, *Pure and applied geophysics* **166**, 1693-1724.

Olsen, H.W. 1962. Hydraulic flow through saturated clays, *Clays and Clay Minerals* **11**(1), 131-161.

Pagano, A. G., Magnanimo, V., Weinhart, T., Tarantino, A. 2020. Exploring the micromechanics of non-active clays by way of virtual DEMexperiments. *Géotechnique*, **70**(4), 303-316.

Pedrotti, M., Tarantino, A. 2018. An experimental investigation into the micromechanics of non-active clays, *Géotechnique* **68**(8), 666-683.

Pennington, D. S., Nash, D. F. T., Lings, M. L. 1997. Anisotropy of G0 shear stiffness in Gault Clay, *Géotechnique* **47**(3), 391-398.

Rice, J.M. 1971. Inelastic constitutive relations for solids: an internal variable theory and its applications to metal plasticity, *J. Mech. Phys. Solids* **19**, 433–455.

Rollo, F., Amorosi, A. 2020. SANICLAY-T: Simple thermodynamic-based anisotropic plasticity model for clays, *Computers and Geotechnics* **127**, 103770.

Rollo, F., Amorosi, A. 2022. Isotropic and anisotropic elastoplastic coupling in clays: a thermodynamic approach. *Int. Journal of Solids and Structures*, 248, 111668.

Rubin, M. B. 2001. Physical reasons for abandoning plastic deformation measures in plasticity and viscoplasticity theory, *Archives of Mechanics*, **53**(4-5), 519-539.

Smart, P., Tovey, N. K. 1982. *Electron microscopy of soils and sediments: techniques*, Oxford University Press, Oxford, UK.

Smart, P. 1969. Soil structure in the electron microscope. *Proceedings, International Conference on Structure, Solid Mechanics Engineering Design Civil Engineering Material*. University of Southampton, United Kingdom.

Smith, P. R., Jardine, R. J., Hight, D. W. 1992. The yielding of Bothkennar clay, *Géotechnique* **42**(2), 257-274.

Terzaghi, K., Peck, R. B. 1948. *Soil mechanics. Engineering Practice*, John Wiley and Sons, New York.

Ulloa, J., Alessi, R., Wambacq, J., Degrande, G., Francois, S. 2021. On the variational modeling of non-associative plasticity. *International Journal of Solids and Structures*, **217**, 272-296.

Yu, C. Y., Chow, J. K., Wang, Y. H. 2016. Pore-size changes and responses of kaolinite with different structures subject to consolidation and shearing, *Engineering Geology* **202**, 122-131.

Zdravkovic, L., Jardine, R. J. 1997. Some anisotropic stiffness characteristics of a silt under general stress conditions, *Géotechnique* **47**(3), 407-437.

Zheng, Y., Baudet, B. A., Delage, P., Pereira, J. M., Sammonds, P. 2022. Pore changes in an illitic clay during one-dimensional compression, *Géotechnique*, 1-16.

Ziegler, H. 1977. *An Introduction to Thermomechanics*, North-Holland, Amsterdam.

Zouain, N., Pontes Filho, I., Borges, L., da Costa, L. M. 2007. Plastic collapse in non-associated hardening materials with application to Cam-clay. *International journal of solids and structures* **44**(13), 4382-4398.

Zouain, N., Pontes, I., Vaunat, J. 2010. Potentials for the modified Cam-Clay model, *European Journal of Mechanics-A/Solids* **29**(3), 327-336.